Identification of HO-1 as a novel biomarker for graft acute cellular rejection and prognosis prediction after liver transplantation

Junjun Jia[1,2,3#], Yu Nie[1,2,3#], Lei Geng[1,2,3], Jianhui Li[1,2,3], Jimin Liu[4], Yifan Peng[2,3], Junjie Huang[2,3], Haiyang Xie[1,2,3], Lin Zhou[1,2,3], Shu-Sen Zheng[1,2,3]

[1]Division of Hepatobiliary and Pancreatic Surgery, Department of Surgery, First Affiliated Hospital, School of Medicine, Zhejiang University, College of Medicine, Hangzhou 310003, China; [2]Key Laboratory of Combined Multi-organ Transplantation, Ministry of Public Health, Hangzhou 310003, China; [3]Collaborative Innovation Centers for Diagnosis Treatment of Infectious Diseases, First Affiliated Hospital, School of Medicine, Zhejiang University, Hangzhou 310003, China; [4]Department of Pathology and Molecular Medicine, Faculty of Health Sciences, McMaster University, Hamilton, Canada

Contributions: (I) Conception and design: J Jia, Y Nie, SS Zheng; (II) Administrative support: L Geng, J Liu, SS Zheng; (III) Provision of study materials or patients: J Jia, Y Nie, J Li, Y Peng, J Huang, H Xie, L Zhou; (IV) Collection and assembly of data: J Jia, Y Nie, L Zhou; (V) Data analysis and interpretation: J Jia, Y Nie, L Geng, J Li; (VI) Manuscript writing: All authors; (VII) Final approval of manuscript: All authors.

[#]These authors contributed equally to this work.

Correspondence to: Prof. Shu-Sen Zheng, MD, PhD, FACS. Key Laboratory of Combined Multi-Organ Transplantation, Ministry of Public Health, Department of Hepatobiliary and Pancreatic Surgery, First Affiliated Hospital of Zhejiang University School of Medicine, 866 Yuhangtang Road, Hangzhou 310003, China. Email: shusenzheng@zju.edu.cn.

Background: Liver transplantation (LT) is the most effective treatment for patients with end-stage liver diseases, but acute rejection is still a major concern. However, the mechanisms underlying rejection remain unclear. Biomarkers are lacking for predicting rejection and long-term survival after LT.

Methods: Isobaric tags for relative and absolute quantitation (iTRAQ)-based proteomics was performed between acute cellular rejection (ACR) and non-rejection recipients. The molecular signature differences and potential biomarkers were identified by comprehensive bioinformatics. Heme oxygenase-1 (HO-1) expression and its association with clinical outcomes were investigated by tissue microarrays consisted of liver specimens from recipients with (n=80) and without ACR (n=57).

Results: A total of 287 differentially expressed proteins (DEPs) were identified. Pathway analysis revealed that T/B cell activation, integrin/inflammation signaling pathway, etc. were significantly correlated with ACR. Through comprehensive bioinformatics, HO-1 was identified as a candidate potential biomarker for ACR. In tissue microarray (TMA) analysis, HO-1 expression was significantly higher in ACR group than in non-rejection group ($P<0.01$). Preoperative Child-Pugh and Meld scores were significantly higher in recipients with high HO-1 expression ($P<0.01$). In a mean 5-year follow-up, recipients with high HO-1 expression were associated with a shorter overall survival ($P<0.05$). Further multivariate analyses indicated that HO-1 could be an independent adverse prognostic factor for post-transplant survival ($P=0.005$).

Conclusions: A total of 287 DEPs were identified, providing a set of targets for further research. Recipients with high preoperative HO-1 expression were associated with ACR. HO-1 may be used as a potential biomarker for predicting the development of post-transplant allograft ACR and recipient's survival.

Keywords: Acute cellular rejection (ACR); heme oxygenase-1 (HO-1); liver transplantation (LT); biomarker

Submitted Oct 05, 2019. Accepted for publication Dec 27, 2019.

doi: 10.21037/atm.2020.01.59

View this article at: http://dx.doi.org/10.21037/atm.2020.01.59

Introduction

Liver transplantation (LT) has been the most effective and widely used treatment for patients with end-stage liver diseases and hepatocellular carcinoma (HCC) fulfilling the selecting criteria. With the improvements in surgical techniques, postoperative management, and immunosuppressive therapies, the long-term outcomes of LT have continued to improve over the last several decades, with 5- and 10-year survival reaching 70% and 60%, respectively (1,2). Despite the advances, acute cellular rejection (ACR) remains the most common and serious complication during early post-transplant period, occurring in 10–40% of patients and potentially leading to irreversible allograft failure (1). Meanwhile, increase use of immunosuppression due to ACR may result in inevitable complications, i.e., infections, metabolic disorders, nephrotoxicity, and ultimately malignancy (3). All the above, would substantially impair life quality, increase morbidity, and reduce long-term survival. Therefore, early identification of patients at risk of developing graft rejection is of paramount importance for saving the graft and increasing the long-term survival. To date, the diagnosis of ACR relies mainly on clinical manifestations and histopathological evidence. However, clinical symptoms like fever, abdominal pain, increasing ascites and laboratory abnormalities in ACR are usually insensitive and nonspecific, which can't reflect the severity of ACR and support the early diagnosis. Liver biopsy remains the gold standard for ACR diagnosis (4), but its expense, inconvenience, susceptibility of sampling error and invasiveness with moderate to severe complications ultimately highlight the need for finding out non-invasive and reliable diagnostic biomarkers for ACR.

Proteomic analysis illuminates a better understanding of biological processes in both healthy and diseased conditions, which has been largely applied to investigate the mechanisms of rejection in organ transplantations (5). Isobaric tags for relative and absolute quantitation (iTRAQ), has become a superior mass-based quantitative proteomic technique by allowing simultaneous identification of protein profiles obtained from multiple and biologically complex samples (6). With the advantages of high-throughput, great accuracy and high sensitivity, iTRAQ has been widely used for systematically characterizing the unique proteomic profile and investigating the molecular mechanisms of human diseases (7). Combined with bioinformatics tools, the data obtained from iTRAQ can be further analyzed and successfully used for identification of novel diagnostic and prognostic biomarkers (8). For instance, Liu *et al.* comprehensively analyzed the proteome characteristics of chronic liver allograft dysfunction (CLAD) in rat models and discovered that targeting CXCL4 protected against the development of CLAD after LT by reducing liver fibrosis (9). However, the combination of iTRAQ-based quantitative proteomics and bioinformatics analysis has rarely been applied to the field of biomarker identification for ACR in LT.

To our knowledge, this is a novel study investigating preoperative protein profile changes and its influence on the prognosis of LT between ACR and non-rejection recipients. This study first aimed to comprehensively characterize the preoperative proteomic alterations among ACR patients using iTRAQ-based proteomics. Combined with bioinformatics analysis, novel potential biomarkers for ACR were identified and then the prognostic value of the identified biomarker were verified by a combination of tissue microarray (TMA) analysis and retrospective cohort study.

Methods

Patients and study design

This study design proceeded by two separate settings (*Figure 1*).

The training set was designed to investigate the proteome differences and to identify potential biomarkers between ACR and non-rejection group. The protein samples extracted from ACR (n=3) and non-rejection recipients (n=3) were analyzed by iTRAQ-based proteomics. Differentially expressed proteins (DEPs) were screened and the potential biomarkers for ACR were identified by comprehensive bioinformatics. For subjects, ACR were confirmed by histological findings according to the Banff criteria (10). All ACR episodes were resolved according to our previous reported protocol (11). Subjects included in non-rejection group were selected based on the following criteria: maintaining stable graft function and lacking rejection signs in the presence of immunosuppressive drugs (IS) for at least 6 months.

The validating set was performed to validate the prognostic value of the candidate biomarker [heme oxygenase-1 (HO-1)] identified in training set by a retrospective study based on a TMA constructed from two independent cohorts: ACR cohort (n=80) and non-rejection

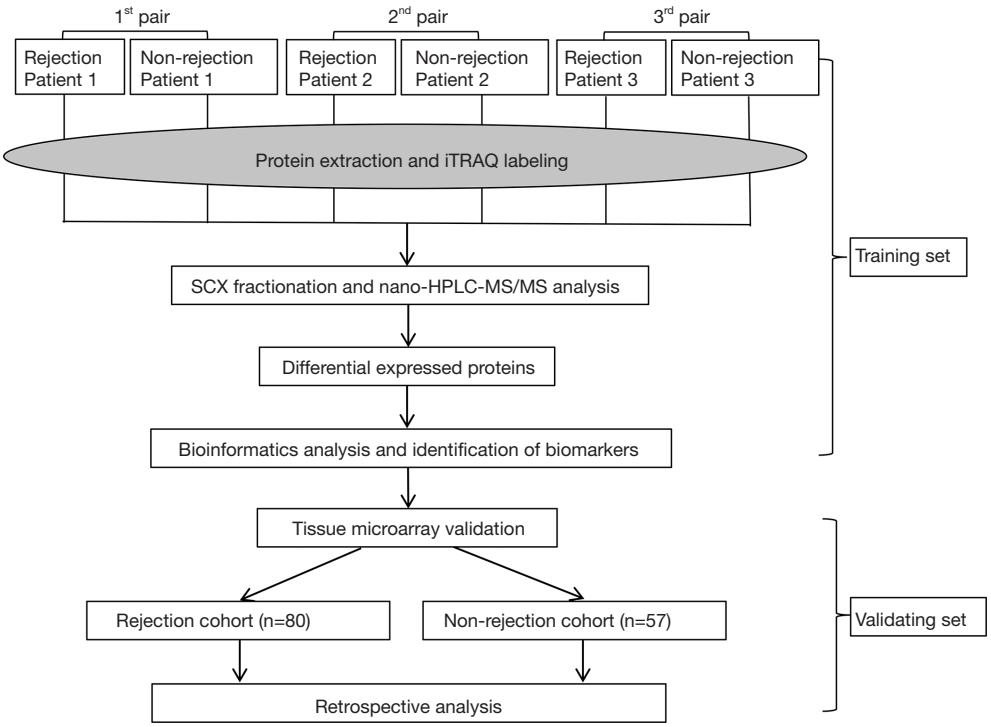

Figure 1 Flowchart of the study design.

cohort (n=57) (*Table 1*). Survival analysis was performed to verify the predictive value of HO-1 for graft rejection. Subjects included in ACR cohort and non-rejection cohort followed the same standards as the training set.

All subjects in this study were included between January 2012 and August 2013 from Department of Hepatobiliary and Pancreatic Surgery, First Affiliated Hospital, Zhejiang University. All subjects met the indications for LT. The pathological diagnosis of ACR of the subjects by needle core liver biopsy was confirmed independently by two experienced pathology experts. The study protocol was approved by the Ethics Committee of The First Affiliated Hospital, School of Medicine, Zhejiang University. No donor liver was from executed prisoners in this study. All recipients were informed with written informed consent for the tissue collection and biopsy.

iTRAQ-based quantitative proteomic study

The detailed protocols for iTRAQ protein identification were listed in Supplementary files.

The DEPs were identified based on following standards: the fold change of protein expression (rejection group *vs.* non-rejection group) was >1.2 for up-regulation and <0.83 for down-regulation, with P<0.05.

Gene ontology (GO) and pathway enrichment analysis

GO annotation, the international standardization of gene function classification system, can provide updating Ontologies, including molecular function, cellular component and biological process, to describe the biological characteristics of large genes and proteins in certain organism (12). In this work, GO enrichment analysis of all DEPs was performed using the Panther Classification System (http://www.pantherdb.org/) (13), compared to the whole human genome. Pathway enrichment analysis was implemented by PANTHER Pathways, which can classify the enriched pathways, providing important information about molecular interactions and reaction networks of the DEPs. P<0.05 was considered statistically significant.

Protein-protein interaction (PPI) network construction

The Search Tool for the Retrieval of Interacting Genes (STRING) database (http://string-db.org) (version 10.0)

Table 1 Demographics and clinical characteristics of patients in HO-1 expression analysis in validation study

Characteristics, n (%)	Rejection (n=80)	Non-rejection (n=57)	P
Age (years)	40.8±9.4	46.4±10.3	P<0.05
Gender			NS
Male	64 (80.0%)	52 (91.2%)	
Female	16 (20.0%)	5 (8.8%)	
Primary diagnosis			NS
HBV cirrhosis	56 (70.0%)	38 (66.7%)	
HCC	14 (17.5%)	11 (19.3%)	
Others	10 (12.5%)	8 (14.0%)	
MELD scores	22.1±10.7	21.4±10.3	NS
Child-Pugh scores	9.7±2.5	9.3±2.4	NS
Serum creatinine (μmol/L)	80.7±60.8	112.5±145.3	NS
ABO compatible (%)	84.30%	81.40%	NS
Time point of rejection (days)	11.2±7.5	–	–

NS, not significant; MELD, model for end stage liver disease.

was used to analyze and visualize the PPI network of the DEPs (14). To exclude false positive interactions as possible, only DEPs with high confidence scores (combined score >0.7) were selected; the sources of interactions were based exclusively on databases and previous experimental results, while excluding other predictions from String (such as gene fusion and text mining). Then, the PPI network was reconstructed and visualized using Cytoscape software (version 3.4.0, http://cytoscape.org/) (15).

Module analysis of the PPI network

To find functional network modules or clusters from PPI network, the module analysis was performed using the Molecular Complex Detection (MCODE) in Cytoscape (16), with a connectivity degree cutoff =2. Then the significant modules with MCODE scores >4 and nodes >10 were selected. The pathway enrichment analysis of the significant modules was performed in Panther system as mentioned above, with P<0.05.

Tissue microarray and immunohistochemical (IHC) staining

The identified candidate protein (HO-1) was validated in two independent cohorts of 137 patients' liver tissues using TMA constructed from formalin-fixed, paraffin embedded tissue blocks. To avoid bias of IHC interpretation, the samples were placed on the TMA blindly. Each sample was arranged in triplicate to avoid tissue loss and tissue heterogeneity. The detailed protocol of IHC staining and intensity scoring was listed in Supplementary Method.

Statistical analysis

Statistical analysis was conducted using SPSS 15.0 software (SPSS, Chicago, IL, USA). Fisher's exact test was used for categorical variables analysis. χ^2 test was used to analyze the immunohistochemical staining results and evaluate the correlation between HO-1 expression and the clinical outcomes. The overall survival was estimated using Kaplan-Meier method and the differences in survival between two groups were compared using the log-rank test. Multivariate analysis was performed using the Cox proportional hazards regression model. P<0.05 was considered statistically significant, with 95% confidence interval (CI).

Results

Demographic and clinical characteristics of patients

In the training set, both ACR and non-rejection group were matched for age, gender and primary diagnosis for protein

identification. Details of the subjects referred to *Table S1*.

For the validating set, two cohorts of patients were included to validate HO-1 identified in the training set. The demographic and clinical characteristics of patients were summarized in *Table 1*. There were no differences in terms of gender, primary diagnosis, Meld scores, Child-Pugh scores, serum creatinine, or ABO compatible between two groups.

Proteomic analysis and identification of the DEPs

The basic information of the proteome profile identified by iTRAQ referred to *Figure S1*. A total of 287 proteins were identified as DEPs finally, including 173 (60.3%) up-regulated proteins and 114 (39.7%) down-regulated proteins among ACR *vs.* non-rejection group. The detailed information of the DEPs was show in *Table S2*.

GO classification analysis of the DEPs

To identify the possible biological and functional properties of 287 DEPs, GO analysis was performed. The results showed different changes in biological characteristics occurred in ACR (*Figure S2*). In the biological process category, up-regulated DEPs were mainly enriched in biological regulation, signaling, immune system process, biological adhesion etc., while down-regulated DEPs were mainly enriched in metabolic process and catabolic process (*Figure S2A*). For molecular function, up-regulated DEPs were mainly observed in catalytic activity, nucleic acid binding and those terms in pathway regulation, while most down-regulated DEPs were more observed in catalytic/transferase/oxidoreductase activity (*Figure S2B*). In brief, up-regulated DEPs were mainly related to the regulation of allograft rejection while down-regulated DEPs may play a greater role in the impaired catabolic and metabolic functions during rejection. As immune system changes were important during ACR, the detailed information of the DEPs involved in this term was summarized in *Table S3*.

Pathway enrichment analysis

To further study the detailed molecular mechanisms of ACR, pathway enrichment analysis was performed. The enriched pathways significantly differed between up- and down-regulated DEPs (*Figure 2*). The mostly enriched pathways in up-regulated DEPs were integrin signaling pathway, Inflammation mediated by chemokine and cytokine signaling pathway, EGF receptor/FGF signaling pathway, T/B cell activation, etc. The down-regulated DEPs were mainly presented in Serine glycine biosynthesis and 5-hydroxytryptamine degradation. Consistent with the GO analysis, up-regulated DEPs were significantly enriched in pathways involved in immune system process and down-regulated DEPs were mainly involved in metabolic pathways.

PPI network analysis of the DEPs

Next, 287 DEPs were summited into STRING database to visualized and analyze the PPI network. Through screening of high confidence interactions (scores >0.7), the PPI network was visualized in *Figure 3*. To better understand the relation between PPI network and protein expression level, the PPI network was reconstructed in Cytoscape (*Figure S3*). The up- and the down-regulated DEPs were clearly demarcated into 2 parts and connected by the interaction between HO-1 (gene symbol: HMOX1) and biliverdin reductase A (BVR) (gene symbol: BLVRA) in PPI network.

Module analysis and pathway enrichment

To identify functional modules from PPI network and find hub-proteins, the top 3 significant functional modules were obtained by module analysis (*Figure S4*). Except for the up-regulated BLVRA, all other proteins in module 1 (18 nodes, MCODE score =4.941) were down-regulated. On the contrary, the vast majority of the proteins in module 2 (30 nodes, MCODE score =4.138) were up-regulated. As for module 3 (10 nodes, MCODE score =4.000), only 40S ribosomal protein S23 (RPS23) was down-regulated.

The module pathway enrichment was then analyzed (*Table S4*). The proteins in module 1 were significantly enriched in metabolic pathways. The proteins in module 2 were significantly enriched in Integrin signaling pathway, B/T cell activation, EGF receptor/FGF signaling pathway, Inflammation mediated by chemokine and cytokine signaling pathway, etc. No significant enrichment was found in module 3 ($P>0.05$).

Module 2, with most proteins up-regulated, accounted for the majority of enrich pathways of 173 up-regulated DEPs (*Table S4*, *Figure 2*), which were mainly about regulation of inflammation and immune system process, suggesting that the activation of module 2 in allograft rejection; The enriched pathways in module 1, with most proteins down-regulated, were mainly involved in metabolic

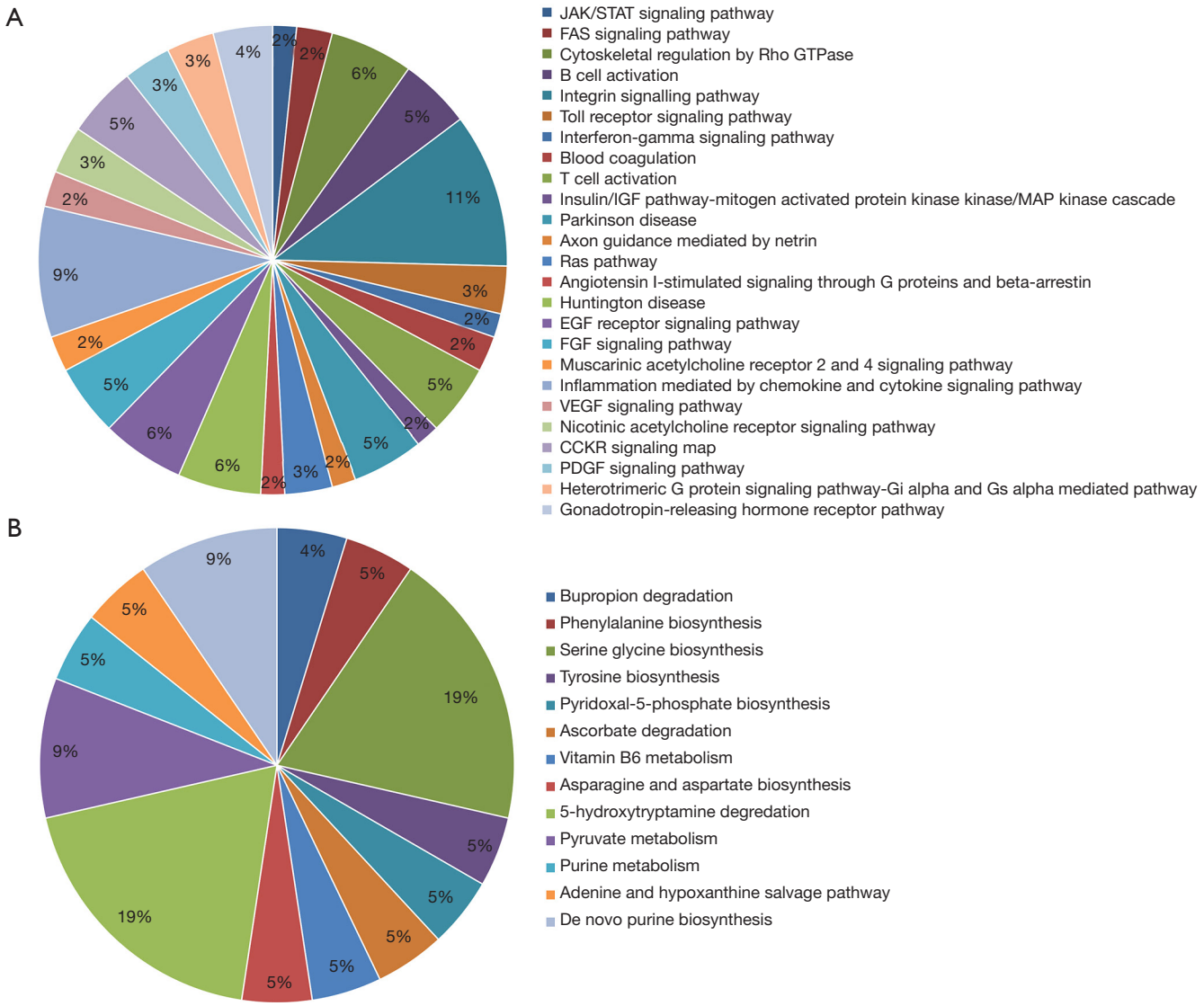

Figure 2 GO pathway analysis of the DEPs associated with allograft rejection. (A) Significantly enriched pathways of up-regulated DEPs. (B) Significantly enriched pathways of down-regulated DEPs. Only significantly enriched pathways (P<0.05) were showed. GO, gene ontology; DEPs, differentially expressed proteins.

process, indicating the inhibition of module 1 during metabolic abnormalities in rejection. Notably, module 1 and module 2 were connected directly by HO-1-BLVRA interaction (*Figures 3*,*S4*). Pathway analysis showed that HIF-1 signaling pathway (including HMOX1, MAPK1, RELA, CUL2) and porphyrin and chlorophyll metabolism (including BLVRA, HMOX1, UGT1A9, UGT2B4) were enriched in the linking part (*Figure 3*). HO-1 was presented in both two enriched pathways in the connection part, indicating the potentially crucial role of HO-1 protein in the regulation of immunoreaction and metabolic function during rejection.

Identification of high HO-1 expression in ACR recipients by TMA analysis

According to the aforementioned results of GO, pathway, module analysis, HO-1 may serve as the key molecule in regulating allograft rejection. Therefore, HO-1 was selected as the candidate protein for further investigation.

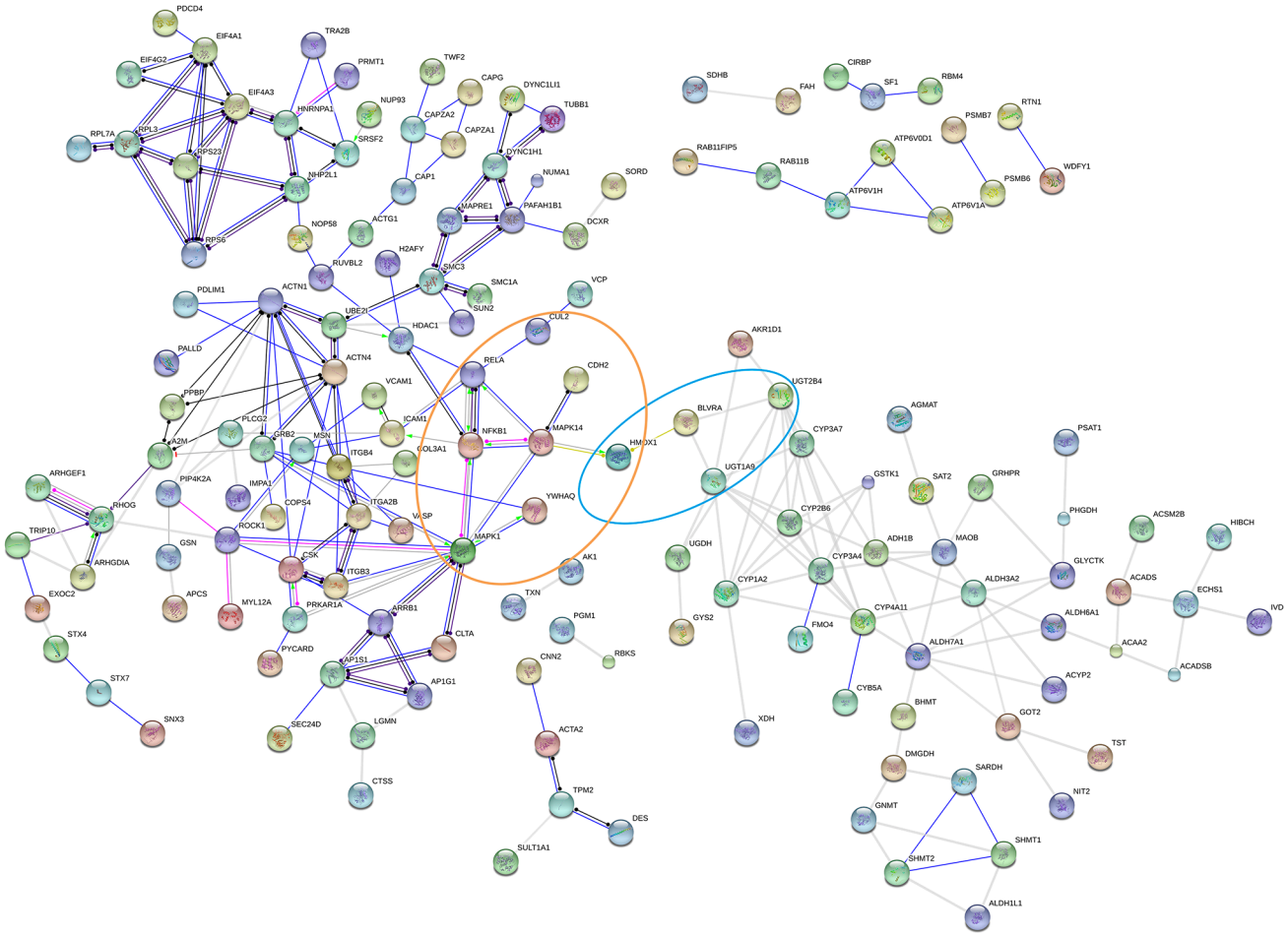

Figure 3 PPI network of DEPs according to the STRING database. The minimum required interaction score was at least 0.7 and only query proteins were visualized, excluding those interactors predicted by String. PPI, protein-protein interaction; DEPs, differentially expressed proteins.

To validate HO-1 expression level and its significance in ACR, HO-1 expression was detected by TMA in two independent cohorts, as described in Methods. The demographic and clinical characteristics of subjects in two cohorts were presented in *Table 1*.

Representative immunohistochemical staining for HO-1 in two cohorts was shown in *Figure 4A*. Statistical analysis of HO-1 expression in TMA showed that in consistent with proteomics quantification, HO-1 expression level was significantly higher in ACR group (n=80) than in non-rejection group (n=57) (*Figure 4B*, P<0.05).

Identification of preoperative HO-1 expression as a potential prognostic factor for ACR

To investigate the association between preoperative HO-1 expression and clinical outcomes, the clinical data of 137 recipients in TMA analysis were reviewed retrospectively. 137 patients were divided into two groups according to HO-1 expression levels (*Table 2*). There was no difference in terms of age, gender and ABO compatible between high and low HO-1 expression group. Notably, significantly higher Child-Pugh and Meld scores were observed in high

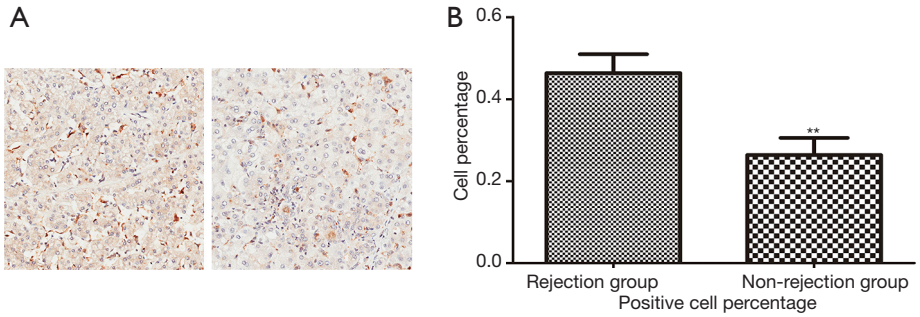

Figure 4 Validation of HO-1 expression in ACR group and non-rejection group by TMA and IHC. (A) Representative images of IHC staining for HO-1 on liver tissue specimens from ACR (n=80) and non-rejection (n=57) recipients (×20). (B) Statistical analysis of HO-1 expression level in rejection and non-rejection group. HO-1 positive cell percentage was significantly higher in rejection group. **, P<0.05. DEPs, differentially expressed proteins; HO-1, heme oxygenase-1; ACR, acute cellular rejection; TMA, tissue microarray; IHC, immunohistochemistry.

Table 2 Characteristics of the recipients between high HO-1 expression group and low HO-1 expression group

HO-1 expression level	high expression (n=41)	low expression (n=96)	P
Age (years)	42.3±1.4	43.4±1.1	NS
Gender (male/female)	34/7	82/14	NS
ABO compatible			NS
Compatible	33	84	
Not compatible	8	12	
Child-Pugh	10.8±0.3	9.0±0.2	<0.01
Meld	26.7±1.7	19.8±0.9	<0.01

NS, not significant.

HO-1 expression group (P<0.01).

To further validate HO-1 expression level as a prognostic factor, overall survival rates were determined using the log-rank test with respect to HO-1 expression level. Kaplan-Meier survival curves based on HO-1 expression level showed that in a 5-year follow-up, high HO-1 expression group had significantly poorer overall survival rate compared with the low HO-1 expression group (P<0.05) (*Figure 5*).

Moreover, multivariate analysis based on the Cox regression model was performed to confirm the pre-operative HO-1 expression as an independent prognostic factor. As showed in *Table 3*, Child-Pugh A was shown to be a protective prognostic factor while age >50 was an unfavourable one. Notably, HO-1 expression was significantly associated with overall survival of LT patients (OR 0.217, P=0.005), suggesting that high preoperative HO-1 expression may be used as an independent, unfavourable prognostic biomarker for predicting the development of post-transplant allograft ACR and recipient's survival.

Discussion

In this study, we systematically compared and characterized the proteome differences of liver tissues between ACR and non-rejection group using iTRAQ-based comparative proteomics. Bioinformatics analysis successfully provided the distinguished molecular signature and critical signaling pathways during ACR. Further TMA analysis and retrospective cohort study showed that preoperative HO-1 expression was significantly higher in ACR patients than in non-rejection patients, which can independently predict the development of post-transplant ACR. HO-1 may serve as a potential biomarker for ACR prognosis.

The field of biomarker identification for liver rejection

is an area of fast-growing interest in recent years. Many studies based on transcriptomics, proteomics and metabolomics have been performed in liver tissue, blood or urine to investigate the molecular signatures in rejection, aiming to find potential biomarkers (17-19). According to the previous studies, proteins related to inflammation are generally up-regulated in rejection graft due to the inflammatory response, while the down-regulated proteins are mainly associated with the disequilibrium of synthetic and metabolic homeostasis during rejection (20,21). As a result, the reported biomarkers are mainly pro-inflammatory and immunoregulatory cytokines, chemokines or other proteins related to inflammation, which showed an increased expression during ACR (21-24). Our differential proteomics study successfully filtered out 287 DEPs. These proteins, consistent with previously published studies, could obviously be divided into 2 distinct clusters: inflammation/immunoregulation-related proteins in up-regulated DEPs; functional proteins mainly involving in metabolic abnormalities in down-regulated DEPs (*Table S2*, *Figure 2*).

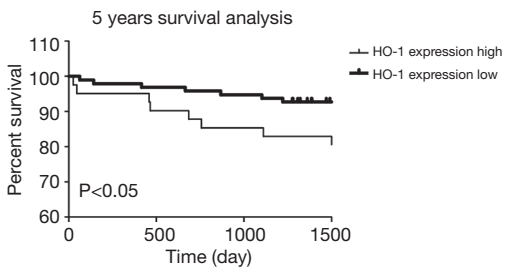

Figure 5 Preoperative high HO-1 expression in liver tissue is associated with poor clinical outcome. High HO-1 expression was defined as HO-1 expression score ≥8. HO-1, heme oxygenase-1.

Further GO and pathway analyses systematically illustrated the visible differences of the molecular signatures between ACR and non-rejection group, reflecting the results of inflammatory reaction and functional abnormality in molecular level during ACR. In a proteomic study based on a CLAD rat model induced from ACR (9), Liu and colleagues found that the DEPs in blood were significantly enriched in B/T cell activation, Integrin signaling pathway, Chemokine signaling pathway, etc., presenting the high overlapping percentage of the enrich pathways with our study, indicating the crucial role of the activation of these pathways in inflammatory reaction during rejection. In another transcriptomic analysis conducted by Lozano *et al.* (25), the enriched pathways in differentially gene transcripts presented the similar pattern, showing enrichment of Integrin pathway, T/B-cell activation, etc. The high degree of similarity in functional pathway enrichment between different studies based on different strategies suggests the important roles of these pathways in the pathogenesis of ACR. Meanwhile, these studies confirm the reliability of our findings in the present work. However, the exact mechanisms underlying the activation of these pathways in ACR remain unclear.

Through module analysis, we identified three important functional modules, especially module 1 and module 2, which accounted for the major enriched pathways in DEPs. Notably, module 2 is relatively more activated, with overwhelming majority of proteins up-regulated, which is the exact opposite in module 1. Proteins in module

Table 3 Multivariate analyses of overall survival in all population of recipients

Variables	B	S.E.	Wald	df	Sig.	Exp (B)
Age, years (>50 *vs.* ≤50)	0.995	0.411	5.855	1	0.016	2.705
Gender (male *vs.* female)	1.048	0.599	3.060	1	0.080	2.852
Serum creatinine (≤130 *vs.* >130)	0.138	0.469	0.087	1	0.769	1.148
ABO compatible	–0.795	0.468	2.889	1	0.089	0.452
MELD scores (≤22 *vs.* >22)	0.751	0.476	2.495	1	0.114	2.119
Child-Pugh status			4.186	2	0.123	
Child-Pugh A	–1.193	0.583	4.186	1	0.041	0.303
Child-Pugh B	–0.515	0.498	1.068	1	0.301	0.598
HO-1 expression (low *vs.* high)	–1.530	0.539	8.040	1	0.005	0.217
Constant	–0.625	0.703	0.792	1	0.374	0.535

2, including NFKB1, MAPK1, MAPK14, RELA, HO-1, ICAM-1, VCAM-1, etc., conferring either pro- or anti-inflammatory effect in inflammation and immune response during ACR, have been reported to be potential biomarkers of liver rejection (18,21). The overexpression of these proteins suggests the excessive activation of the NF-κB and MAPK related inflammatory pathway. It may increase the expression of many inflammatory cytokines and chemokines in liver tissue or blood, which will be centrally involved in the activation of T cell immunity (26). Thus, preoperatively excessive activation of inflammatory pathways may exist in ACR patients and cause high levels of inflammatory cytokines in circulation, which may lead to allograft function abnormalities and post-transplantation rejection (27). For instance, the overexpression of ICAM-1 and VCAM-1 in serum or liver tissues, may facilitate the adhesion and extravasation of activated immune cells from the circulation into liver, thus magnifying the inflammation during ACR (18). Nonetheless, the exact mechanism underlying the up-regulation of these proteins at the point of ACR remains unknown and needs to be evaluated in further researches.

HO-1, the rate-limiting enzyme in heme catabolism, can catalyze heme to free iron, carbon monoxide (CO), and biliverdin (subsequently reduced to bilirubin by biliverdin reductase). Under various stressful stimuli like hypoxia, reactive oxygen species (ROS), and inflammation, HO-1 can be rapidly induced to confer cytoprotective functions through various biological processes, including antioxidant, maintaining microcirculation, preventing ischemia/reperfusion injury, anti-inflammation, immunoregulation, etc. (28). In LT setting, accumulating evidences have previously demonstrated up-regulated HO-1 expression during rejection, which may protect liver grafts against rejection and improve graft survival (29). In present study, HO-1's critical role in PPI network suggested its importance in immunoregulation and liver metabolism during ACR. However, contrary to many aforementioned protective roles of HO-1 overexpression against rejection, our study showed relative overexpression of HO-1 in ACR subjects rather than non-rejection subjects and preoperatively exaggerated HO-1 expression significantly correlated with poorer 5-year overall survival. Though the exact mechanisms explaining this clinical observation remain unknown, we indeed found preoperative high HO-1 an independent adverse predictor for ACR instead of a protective one. More studies are needed to clarify this issue.

To our knowledge, this is the first study that confirms significant higher HO-1 expression in tissue level in ACR recipients compared to non-rejection recipients before transplantation. Similar observations have been made by several studies. Eisuke etc. observed significantly higher serum HO-1 levels in patients with more severe liver injury (30). In a study of 380 patients undergoing non-cardiac surgery, Zheng *et al.* reported preoperative serum HO-1 were significantly higher in patients with adverse cardiac events than in the controls, and higher preoperative HO-1 level was associated with the severity of postoperative adverse cardiac events (OR 1.30, P=0.002) (31). Contrary to our past views about HO-1's protective roles, deliberately induced HO-1 overexpression may increase postoperative liver injury, as shown by aggravation of ALT level, cell necrosis and ferroptosis (32,33). In the donor setting, preoperative excessive HO-1 expression was also believed to be associated with postoperative rejection or early graft dysfunction. Using a lung transplantation model of rat, Bonnell *et al.* found that HO-1 expression levels progressively increased with time and with severity of ACR (34). In a prospective study, excessive preoperative HO-1 expression significantly correlated with post-transplant graft injury and poorer hepatobiliary function, which showed higher postoperative serum AST/ALT levels and worse bile excretion in high HO-1 expression recipients (35). Positive correlation between HO-1 expression and postoperative serum ALT levels seen in these studies suggested that HO-1 levels may partly reflect the severity of preoperative liver injury.

In this study, higher Child-Pugh scores and Meld scores before transplant were observed in recipients with high HO-1 expression (*Table 2*), indicating that patients in high HO-1 expression group presented poorer liver function. To be noted, better Child-Pugh status was found to be a favourable factor for LT prognosis in multivariate analyses (*Table 3*). There are studies reporting that worse MELD scores were associated postoperative graft dysfunction and poor prognosis (36,37). Therefore, we speculate that exaggerated HO-1 activity before transplant may reflect the excessive liver injuries in recipients, which can lead to more severe postoperative early graft dysfunction.

One explanation for the lack of graft protection seen with preoperative high HO-1 expression in our study is that apart from donor's factor, pre-operative overall state of recipients can also provide important contributions to post-operative graft function. The recipients' underlying illness and pre-operative condition may alter the levels of inflammatory and/or immunologically associated proteins in circulation.

Preoperatively excessive activation of inflammatory pathways, as shown in our pathway analysis, may exist in ACR patients, causing high levels of inflammatory cytokines or immune injury-associated proteins in circulation (26,27), which, in return, may be detrimental to postoperative allograft function by aggravating inflammatory injuries in allograft and thus causing postoperative ACR. Theoretically, the more severe the pre-operative illness is, the more HO-1 may be induced to protect cells. Thus, it is quite reasonable to observe that pre-operative higher HO-1 expression was associated with higher rate of postoperative rejection and poorer survival.

Another possibility is that excessive HO-1 expression may aggravate the pre-operative illness instead of providing cytoprotection. Exaggerated HO-1 expression may sensitize cells to oxidative stress due to an accumulation of free iron, thereby resulting in a pro-oxidant condition and increasing postoperative oxidative injury (33,38). HO-1 overexpression may also aggravate the activation of macrophage, the main source of pro-inflammatory mediators in liver, thus increasing the releasing of ROS, TNF-α, TGF-β, etc. into circulation, which in return, may exacerbate postoperative immunoreaction and inflammation in the graft (39,40). However, we were unable to clarify the controversial effects of high HO-1 expression of either cytoprotection or increased cytotoxicity in grafts in this study. Further studies will be necessary to elucidate the clinical implications of HO-1 expression in detail.

In their serial studies, Nakamura etc. reported that post-transplant high HO-1 could regulate macrophage activation and sterile inflammation during I/R injury; and post- but not pre-transplant high HO-1 expression correlated with better hepatic function in human OLT (41,42). Notably, they also found that pre-transplant high and post-transplant low HO-1 expression trended with inferior overall survival (43). Post-transplant low macrophage HO-1 expression in human liver grafts correlated with a 40% reduced 3-year survival rates, indicating recipient HO-1 inducibility is essential for posttransplant hepatic HO-1 expression and its graft protective roles. Combining their results with our data, whether the combination of pre-transplant and post-transplant HO-1 expression will offer better predictive value deserves further researches.

There are several inherent limitations in this study. A limitation is the patients' background. Different individual patients might have different genetic and pathological backgrounds. Though we matched the underlying diseases between ACR and non-rejection groups, the distinguished proteome profile and the HO-1 expression level between two groups may be affected by different individual background. Second, rejection is the result of the immune reactions between recipients and the donor liver. However, only the recipient's HO-1 expression was examined and the influences of donor's HO-1 expression were not investigated. In addition, whether combination of the recipient's and donor's HO-1 will offer better predictive value deserves further researches. The third limitation is the relatively small sample size, especially in training set. Though we included two cohorts in validating set to increase the sample volume and to guarantee the reliability of the research findings, HO-1's predicting value needs to be confirmed in large multicenter prospective trials and further studies are also needed to investigate remaining potential biomarker candidates in DEPs list.

Conclusions

In summary, our study confirmed a list of 287 DEPs and systematically characterized the preoperative proteome differences in the episode of ACR, providing a set of potential targets for future investigation into the molecular mechanisms and biomarkers. Preoperative high HO-1 expression was validated in tissue level and was identified as a potential biomarker for predicting the development of post-transplant ACR and recipient's survival. However, HO-1's roles in ACR must be confirmed in larger cohort studies. Further studies could be performed to verify additional candidate biomarkers in the data set, which may eventually help develop more efficient diagnostic tools and treatment targets for ACR.

Acknowledgments

Funding: This work was supported by Foundation for Innovative Research Groups of the National Natural Science Foundation of China (No. 81421062), National Natural Science Foundation of China (No. 81470891/81373160), Special Grant from China Postdoctoral Science Foundation (2019T120525), China Postdoctoral Science Foundation (2017M610374), Zhejiang Health Technology Project (2019RC153), and Fundamental Research Funds for the Central Universities (2018FZA7003). The funders had no role in study design, data collection and analysis, decision to publish, or preparation of the manuscript.

Footnote

Conflicts of Interest: The authors have no conflicts of interest to declare.

Ethical Statement: The authors are accountable for all aspects of the work in ensuring that questions related to the accuracy or integrity of any part of the work are appropriately investigated and resolved. The study protocol was approved by the ethics committee review board of the First Affiliated Hospital, Zhejiang University. Informed consent was obtained from all patients for surgical treatment.

References

1. Adams DH, Sanchez-Fueyo A, Samuel D. From immunosuppression to tolerance. J Hepatol 2015;62:S170-85.
2. Sapisochin G, Bruix J. Liver transplantation for hepatocellular carcinoma: outcomes and novel surgical approaches. Nat Rev Gastroenterol Hepatol 2017;14:203-17.
3. Emond JC, Griesemer AD. Tolerance in clinical liver transplantation: The long road ahead. Hepatology 2017;65:411-3.
4. Demetris AJ, Bellamy C, Hubscher SG, et al. 2016 Comprehensive Update of the Banff Working Group on Liver Allograft Pathology: Introduction of Antibody-Mediated Rejection. Am J Transplant 2016;16:2816-35.
5. Xu M, Tan C, Hu J, et al. Expression of hemopexin in acute rejection of rat liver allograft identified by serum proteomic analysis. Shock 2014;42:65-74.
6. Wiese S, Reidegeld KA, Meyer HE, et al. Protein labeling by iTRAQ: a new tool for quantitative mass spectrometry in proteome research. Proteomics 2007;7:340-50.
7. Qian Y, Yao W, Yang T, et al. aPKC-iota/P-Sp1/Snail signaling induces epithelial-mesenchymal transition and immunosuppression in cholangiocarcinoma. Hepatology 2017;66:1165-82.
8. Wong YK, Zhang J, Hua ZC, et al. Recent advances in quantitative and chemical proteomics for autophagy studies. Autophagy 2017;13:1472-86.
9. Li J, Liu B, Shi Y, et al. CXCL4 Contributes to the Pathogenesis of Chronic Liver Allograft Dysfunction. J Immunol Res 2016;2016:9276986.
10. Haas M, Sis B, Racusen L, et al. Banff 2013 meeting report: Inclusion of c4d-negative antibody-mediated rejection and antibody-associated arterial lesions. Am J Transplant 2014;14:272-83.
11. Shen T, Lin BY, Jia JJ, et al. A modified protocol with rituximab and intravenous immunoglobulin in emergent ABO-incompatible liver transplantation for acute liver failure. Hepatobiliary Pancreat Dis Int 2014;13:395-401.
12. Consortium GO. Gene ontology consortium: going forward. Nucleic Acids Res 2015;43:D1049-56.
13. Mi H, Huang X, Muruganujan A, et al. PANTHER version 11: expanded annotation data from Gene Ontology and Reactome pathways, and data analysis tool enhancements. Nucleic Acids Res 2017;45:D183-9.
14. Szklarczyk D, Morris JH, Cook H, et al. The STRING database in 2017: quality-controlled protein–protein association networks, made broadly accessible. Nucleic Acids Res 2017;45:D362-8.
15. Bader GD, Hogue CW. An automated method for finding molecular complexes in large protein interaction networks. BMC bioinformatics 2003;4:2.
16. Saito R, Smoot ME, Ono K, et al. A travel guide to Cytoscape plugins. Nat Methods 2012;9:1069-76.
17. Sarwal MM. Fingerprints of transplant tolerance suggest opportunities for immunosuppression minimization. Clin Biochem 2016;49:404-10.
18. Germani G, Rodriguez-Castro K, Russo FP, et al. Markers of acute rejection and graft acceptance in liver transplantation. World J Gastroenterol 2015;21:1061.
19. Baroja-Mazo A, Revilla-Nuin B, Parrilla P, et al. Tolerance in liver transplantation: Biomarkers and clinical relevance. World J Gastroenterol 2016;22:7676.
20. Brunet M, Shipkova M, van Gelder T, et al. Barcelona consensus on biomarker-based immunosuppressive drugs management in solid organ transplantation. Ther Drug Monit 2016;38:S1-S20.
21. Verhelst XP, Troisi RI, Colle I, et al. Biomarkers for the diagnosis of acute cellular rejection in liver transplant recipients: A review. Hepatol Res 2013;43:165-78.
22. Okubo K, Wada H, Tanaka A, et al. Identification of Novel

and Noninvasive Biomarkers of Acute Cellular Rejection After Liver Transplantation by Protein Microarray. Transplant Direct 2016;2:e118.
23. Bonaccorsi-Riani E, Pennycuick A, Londoño MC, et al. Molecular characterization of acute cellular rejection occurring during intentional immunosuppression withdrawal in liver transplantation. Am J Transplant 2016;16:484-96.
24. Massoud O, Heimbach J, Viker K, et al. Noninvasive diagnosis of acute cellular rejection in liver transplant recipients: A proteomic signature validated by enzyme-linked immunosorbent assay. Liver Transpl 2011;17:723-32.
25. Lozano JJ, Pallier A, Martinez-Llordella M, et al. Comparison of Transcriptional and Blood Cell-Phenotypic Markers Between Operationally Tolerant Liver and Kidney Recipients. Am J Transplant 2011;11:1916-26.
26. Sun B, Karin M. NF-κB signaling, liver disease and hepatoprotective agents. Oncogene 2008;27:6228-44.
27. Friedman BH, Wolf JH, Wang L, et al. Serum cytokine profiles associated with early allograft dysfunction in patients undergoing liver transplantation. Liver Transpl 2012;18:166-76.
28. Zhang M, Nakamura K, Kageyama S, et al. Myeloid HO-1 modulates macrophage polarization and protects against ischemia-reperfusion injury. JCI Insight 2018. doi: 10.1172/jci.insight.120596.
29. Ryter SW, Choi AM. Targeting heme oxygenase-1 and carbon monoxide for therapeutic modulation of inflammation. Transl Res 2016;167:7-34.
30. Ozawa E, Abiru S, Nagaoka S, et al. Ferritin/alanine aminotransferase ratio as a possible marker for predicting the prognosis of acute liver injury. J Gastroenterol Hepatol 2011;26:1326-32.
31. Zheng H, Ma HP, Wang J, et al. Preoperative HO-1 levels as prognostic factor for adverse cardiac events in elder patients undergoing non-cardiac surgery. PLoS One 2013;8:e58567.
32. Froh M, Conzelmann L, Walbrun P, et al. Heme oxygenase-1 overexpression increases liver injury after bile duct ligation in rats. World J Gastroenterol 2007;13:3478.
33. Fang X, Wang H. Ferroptosis as a target for protection against cardiomyopathy. Proc Natl Acad Sci U S A 2019;116:2672-80.
34. Bonnell MR, Visner GA, Zander DS, et al. Heme-oxygenase-1 expression correlates with severity of acute cellular rejection in lung transplantation. J Am Coll Surg 2004;198:945-52.
35. Geuken E, Buis CI, Visser DS, et al. Expression of Heme Oxygenase-1 in Human Livers Before Transplantation Correlates with Graft Injury and Function After Transplantation. Am J Transplant 2005;5:1875-85.
36. Roth JA, Chrobak C, Schädelin S, et al. MELD score as a predictor of mortality, length of hospital stay, and disease burden: A single-center retrospective study in 39,323 inpatients. Medicine 2017;96:e7155.
37. Bruns H, Lozanovski VJ, Schultze D, et al. Prediction of postoperative mortality in liver transplantation in the era of MELD-based liver allocation: a multivariate analysis. PLoS One 2014;9:e98782.
38. Drummond GS, Baum J, Greenberg M, et al. HO-1 overexpression and underexpression: Clinical implications. Arch Biochem Biophys 2019;673:108073.
39. Fahrner R, Dondorf F, Ardelt M, et al. Role of NK, NKT cells and macrophages in liver transplantation. World J Gastroenterol 2016;22:6135.
40. Vijayan V, Wagener F, Immenschuh S. The macrophage heme-heme oxygenase-1 system and its role in inflammation. Biochem Pharmacol 2018;153:159-67.
41. Nakamura K, Kageyama S, Yue S, et al. Heme oxygenase-1 regulates sirtuin-1-autophagy pathway in liver transplantation: From mouse to human. Am J Transplant 2018;18:1110-21.
42. Nakamura K, Zhang M, Kageyama S, et al. Macrophage heme oxygenase-1-SIRT1-p53 axis regulates sterile inflammation in liver ischemia-reperfusion injury. J Hepatol 2017;67:1232-42.
43. Kageyama S, Hirao H, Nakamura K, et al. Recipient HO-1 inducibility is essential for posttransplant hepatic HO-1 expression and graft protection: From bench-to-bedside. Am J Transplant 2019;19:356-67.

Cite this article as: Jia J, Nie Y, Geng L, Li J, Liu J, Peng Y, Huang J, Xie H, Zhou L, Zheng SS. Identification of HO-1 as a novel biomarker for graft acute cellular rejection and prognosis prediction after liver transplantation. Ann Transl Med 2020;8(5):221. doi: 10.21037/atm.2020.01.59

Protein preparation for iTRAQ analysis

Fresh liver tissues were collected from recipients' explant liver intraoperatively and immediately preserved at –80 ℃ for further iTRAQ analysis. The fresh explant tissues were taken and fixed in 10% formalin for tissue microarray in validation set.

Liver tissues from three paired rejection and non-rejection recipients were respectively homogenized to powder in liquid nitrogen and then lysed with Lysis buffer A (7 M Urea, 2 M Thiourea, 4% CHAPS, 40 mM Tris-HCl, pH 8.5; 1mM PMSF and 2mM EDTA), followed by adding of 10 mM DTT 5 min later, sonication at 200 W for 15 min and then centrifugation at 4 ℃, 30,000 ×g for 15 min. The supernatant was precipitated with chilled acetone (5× volume, containing 10% TCA) and incubated at –20 ℃ overnight. After centrifugation, the pellet was rinsed with chilled acetone three times and air dried. The pellet was dissolved in Lysis buffer B (7 M urea, 2 M thiourea, 4% NP40, 20 mM Tris-HCl, pH 8.0–8.5), sonicated at 200 W for 15 min and centrifuged at 4 ℃, 30,000 ×g for 15 min. The supernatant was then transferred to the fresh tube, reduced using 10 mM DTT at 56 ℃ for 1 h, and alkylated with 55 mM IAM in the darkroom for 1 h. After being precipitated with chilled acetone (5× volume) at –20 ℃ for 2 h and centrifuged at 4 ℃, 30,000 ×g for 15 min, the protein sample was air-dried and resuspended in 500 μL 0.5 M TEAB (Applied Biosystems, Milan, Italy), sonicated at 200 W for 15 min and centrifuged as describe above. Finally, the proteins in the supernatant were quantified using Bradford assay (Bio-Rad Laboratories, CA, USA) and stored at –80 ℃ for further analysis.

iTRAQ labeling and SCX fractionation

Pooled proteins (100 μg) from each sample solution were digested overnight with Trypsin Gold (Promega, Madison, WI, USA) with the ratio of trypsin: protein 1:30 at 37 ℃, followed by a vacuum centrifugation for drying. Next, peptides were reconstituted in 0.5 M TEAB and processed with the iTRAQ-8plex kit (Applied Biosystems SCIEX, USA) following the manufacture's protocol. Briefly, samples were labeled with the iTRAQ tags as follows: the rejection group samples were labeled with 118, 119 and 121 iTRAQ tags respectively, and the non-rejection group samples were labeled with 113, 115 and 117 iTRAQ tags (*Figure 1*). After incubation at room temperature for 2 h, the labeled samples were pooled together, dried by vacuum centrifugation, and subjected to fractionation. To avoid the labeling bias, two independent biological replicates were used and three independent replicate experiments were performed.

Strong cation exchange (SCX) chromatography was performed to clean and fractionate the labeled samples using LC-20AB HPLC Pump system (Shimadzu, Kyoto, Japan). Briefly, the iTRAQ-labeled peptide mixtures were reconstituted in 4 mL buffer A (25 mM NaH_2PO_4 in 25% ACN, pH 2.7) and then loaded onto a 4.6 mm × 250 mm Ultremex SCX column with 5 μm particles (Phenomenex). The peptides were eluted according to following procedures: flow rate 1 mL/min; a gradient of buffer A for 10 min, 5–60% buffer B (25 mM NaH2PO4, 1 M KCl in 25% ACN, pH 2.7) for 27 min, 60–100% buffer B for 1 min and maintenance at 100% for 1 min, equilibrium with buffer A for 10 min; monitoring the absorbance at 214 nm; fractions collected every 1 min. The eluted peptides were pooled into 20 fractions and desalted with a Strata X C18 column (Phenomenex) before vacuum-drying.

High-performance liquid chromatography-tandem mass spectrometry (HP LC-MS/MS)

The SCX fractions were first separated by nanoHPLC and then analyzed by tandem mass spectrometry (MS/MS). Briefly, each fraction was re-dissolved in buffer A (5% ACN, 0.1% FA), followed by being centrifuged at 20,000 ×g for 10 min. Using a LC-20AD nanoHPLC (Shimadzu, Kyoto, Japan), 10 μL of peptide sample was loaded onto a 2 cm C18 trap column with a flow rate of 8 μL/min for 3 min and was then gradiently eluted by buffer B (95% ACN, 0.1% FA) on a 10 cm analytical C18 column (inner diameter 75 μm) packed in-house with the following procedures: flow rate 0.3 μL/min, 5% buffer B for 1 min, a gradient from 5% to 35% buffer B for 35 min, a 5 min linear gradient to 60%, a 2 min linear gradient to 80% and maintenance for 4 min. Finally, the system returned to 5% buffer B in 1 min and was maintained at 5% for 10 min.

The LC eluted peptides were analyzed by TripleTOF 5600 System (AB SCIEX, Concord, ON) fitted with a Nanospray III source (AB SCIEX, Concord, ON) and a SilicaTip emitter (New Objectives, Woburn, MA). The key parameters of data acquisition included: ion spray voltage 2.5 kV, curtain gas 30psi, nebulizer gas 15psi, interface heater temperature 150 ℃; resolving power (R.P.) of TOF MS scans: ≥ 30 kF WHM; information-dependent acquisition (IDA): survey scans 250 ms, charge state from 2+ to 5+, up to 30 MS/MS spectra acquired per cycle,

minimum threshold 120 counts/s, total cycle time: fixed to 3.3 s; Q2 transmission 100 Da for 100%; four time bins summed for each scan, pulse frequency value 11 kHz, monitoring of the 40 GHz multichannel TDC detector with four-anode channel detect ion; collision-induced dissociation setting: sweeping collision energy 35±5 eV, iTRAQ adjust rolling collision energy for all precursor ions; dynamic exclusion: 1/2 of peak width (15 s).

Data analysis

Raw data files obtained from the iTRAQ were converted into MGF format files using Proteome Discoverer 1.2 (PD 1.2, Thermo). Mascot software (version 2.3.02, Matrix Science Inc., MA, USA) was used for proteins identification by searching against UniProt/SwissProt Homo sapiens database (2019_06, with 20,431 reviewed entries), with the false discovery rate (FDR) <1%. The key search parameters were set as follows: (I) type of search-MS/MS Ion search, charge states of peptides: +2 and +3; (II) the enzyme specificity of trypsin; (III) max missed cleavages: 1; (IV) the parent ion mass tolerance: 10 ppm, fragment ion mass tolerance: 0.5 Da; (V) the potential variable modifications: Gln > pyro-Glu (N-term Q), oxidation (M), deamidated (NQ); (VI) fixed modifications: carbamidomethyl (C), iTRAQ8plex (N-term), iTRAQ8plex (K). To reduce the probability of false peptide identification, only peptides with significance scores (≥20), FDR <1% and protein probability >99.0% were accepted. Each identified confident protein included at least one unique peptide. For protein quantitation, the Student's *t*-test was used for statistical analysis and the relative quantitation of a given protein was reported as the median ratio in Mascot. $P<0.05$ was considered statistically significant.

Immunohistochemical (IHC) staining for tissue microarray

Tissue microarray sections were immunohistochemically stained for HO-1 to evaluate its expression level. In brief, TMA slides were deparaffinized in xylene and rehydrated in graded alcohols for 5 min, and then immersed in citrate buffer (pH 6.1) at 95 ℃ for antigen retrieval for 40 min. The slides were blocked for endogenous peroxidase activity in 0.3% hydrogen peroxide for 20 min. After washing and incubation overnight at 4 ℃ with primary antibodies against HO-1 (1:600 dilution, Abcam, USA), the slides were incubated with rabbit anti-HO-1 at room temperature for 30 min. Following several washing steps, the slides were immersed for 10 minutes using diaminobenzidine as the chromogen and then counterstained with hematoxylin for 5 minutes. The slides were scanned and visualized using the Aperio ScanScope XT (Aperio) to generate high-resolution digital images for evaluating the stained data.

HO-1 expression levels were evaluated semiquantitatively by the staining intensity combined with the percent of positively stained cells. The staining intensity of HO-1 (intensity scores) was scored as: 0 (negative); 1 (weak); 2 (moderate), and 3 (strong). The percentages of positive cells per field (percent positivity scores) were scored as: 1 (<25%), 2 (25% to 50%), 3 (50% to 75%), 4 (>75%). The overall HO-1 expression score was calculated according to the following formula: intensity score × percent positivity score, which ranged from 0 to 12. Therefore, HO-1 expression can be defined as low expression (HO-1 expression score <8) and high expression (HO-1 expression score ≥8).

Two pathologists, blinded to this study, independently evaluated and scored each case. Differences in interpretation were settled by the consensus.

Table S1 The clinical characteristics of ACR and non-rejection patients for iTRAQ protein identification

Characteristics	Rejection group			Non-rejection group		
	Patient 1	Patient 2	Patient 3	Patient 1	Patient 2	Patient 3
Age (years)	56	54	34	51	48	38
Gender	Female	Female	Male	Female	Male	Male
Diagnosis	Cirrhosis-HBV	Cirrhosis-HBV	Cirrhosis-HBV	Cirrhosis-HBV	Cirrhosis-HBV	Cirrhosis-HBV
Time for rejection after LT (days)	35	24	13	–	–	–

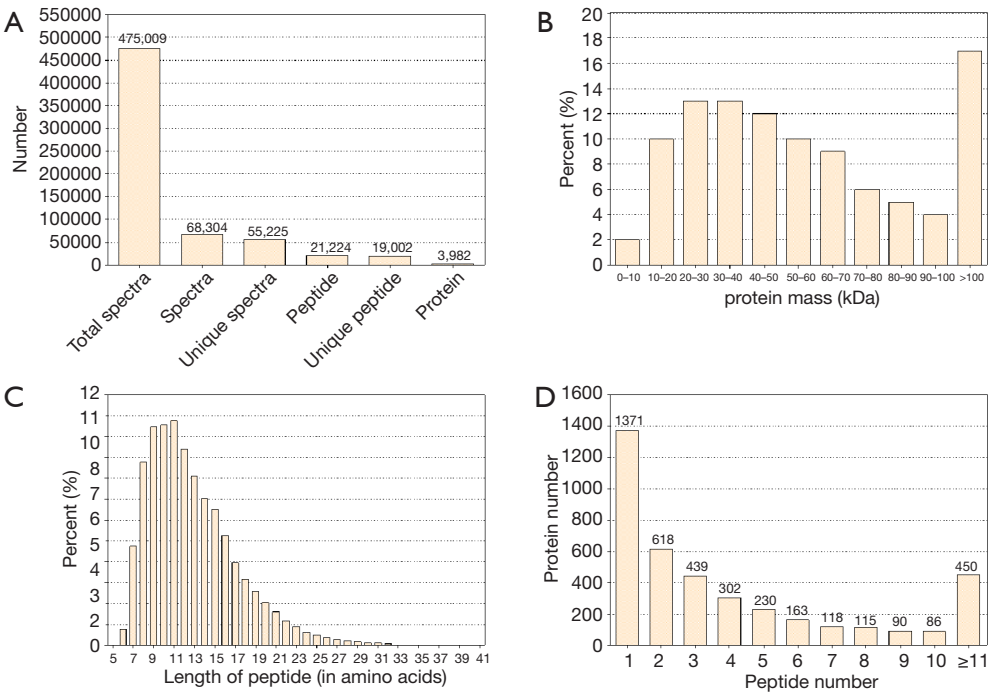

Figure S1 Basic information of the proteome profile identified by iTRAQ. (A) Spectra, peptides and proteins identified from iTRAQ. Spectra are the total numbers of the secondary mass spectrums matching to the known spectra. Unique spectra are the numbers of spectrums matching to the unique peptide. Unique Peptide is the identified peptides specifically belonging to a group of proteins, and Protein is the finally identified proteins. A total of 475,009 spectrums and 21,224 peptides were obtained. Among these, 68,304 spectrums were matched to the known spectrums and 55,255 unique spectrums were matched to 19,002 unique peptides. Finally, 3,982 proteins were identified. (B) Protein mass distribution. (C) Unique peptide length (in amino acids) distribution. (D) Unique peptide number distribution. About 95% of the proteins are in 7–22 amino acids length and over 65% of the proteins included at least two peptides.

Table S2 List of DEPs identified by iTRAQ in training set

UniProt accession	Protein names	Gene symbols	Fold change
Up-regulated proteins			
P02775	Pro-platelet basic protein	PPBP	6.243
Q9H4B7	Tubulin beta 1 class VI	TUBB1	5.044
P05106	Integrin subunit beta 3	ITGB3	3.996
Q9BQI0	Allograft inflammatory factor 1-like	AIF1L	3.582
P13224	Isoform 2 of Platelet glycoprotein Ib beta chain	GP1BB	3.535
P08514	Integrin subunit alpha-Iib	ITGA2B	2.952
Q96JY6	Isoform 5 of PDZ and LIM domain protein 2	PDLIM2	2.822
Q14019	Coactosin like F-actin binding protein 1	COTL1	2.331
P31146	Coronin 1A	CORO1A	2.179
Q9BXF6	RAB11 family interacting protein 5	RAB11FIP5	2.158
P68871	Hemoglobin subunit beta	HBB	2.111
Q9BUP0	EF-hand domain family member D1	EFHD1	2.009
P19320	Vascular cell adhesion molecule 1	VCAM1	1.994
P08575	Receptor-type tyrosine-protein phosphatase C	PTPRC	1.950
O60234	Glia maturation factor gamma	GMFG	1.936
Q8WYJ6	Septin 1	SEPT1	1.906
P08637	Fc fragment of IgG receptor IIIa	FCGR3A	1.899
O75367	H2A histone family member Y	H2AFY	1.890
Q16799	Reticulon 1	RTN1	1.887
P50552	Vasodilator-stimulated phosphoprotein	VASP	1.887
Q8TD55	Pleckstrin homology domain containing O2	PLEKHO2	1.870
Q8WWQ8	Stabilin 2	STAB2	1.848
P84095	Rho-related GTP-binding protein RhoG	RHOG	1.828
Q8WX93	Palladin, cytoskeletal associated protein	PALLD	1.806
P16144	Integrin subunit beta 4	ITGB4	1.801
P17661	Desmin	DES	1.770
Q53EL6	Programmed cell death 4 (neoplastic transformation inhibitor)	PDCD4	1.767
Q9H4G4	Golgi-associated plant pathogenesis-related protein 1	GLIPR2	1.716
Q9UHY1	Nuclear receptor-binding protein	NRBP1	1.702
P09601	Heme oxygenase 1	HMOX1	1.700
P48681	Nestin	NES	1.683
P61225	Ras-related protein Rap-2b	RAP2B	1.668
O15400	Syntaxin 7	STX7	1.655
P20036	Major histocompatibility complex, class II, DP alpha 1	HLA-DPA1	1.643
P62993	Growth factor receptor-bound protein 2	GRB2	1.632
Q03518	Transporter 1, ATP binding cassette subfamily B member	TAP1	1.632
Q9NUQ9	Protein FAM49B	FAM49B	1.630
O75923	Isoform 10 of Dysferlin	DYSF	1.625
P62942	Peptidyl-prolyl cis-trans isomerase	FKBP1A	1.620
Q92522	H1 histone family member X	H1FX	1.615
Q14011	Cold-inducible RNA-binding protein	CIRBP	1.615
Q9NR12	PDZ and LIM domain protein 7	PDLIM7	1.591
O15145	Actin-related protein 2/3 complex subunit 3	ARPC3	1.578
Q6PIU2	Neutral cholesterol ester hydrolase 1	NCEH1	1.576
O94919	Endonuclease domain containing 1	ENDOD1	1.568
P24557	Thromboxane A synthase 1	TBXAS1	1.567
P53396	ATP citrate lyase	ACLY	1.563
P06396	Gelsolin	GSN	1.563
P39023	60S ribosomal protein L3	RPL3	1.557
P63261	Actin, cytoplasmic 2	ACTG1	1.554
Q99538	Legumain	LGMN	1.552
Q9Y3L3	SH3 domain binding protein 1	SH3BP1	1.552
P41240	C-src tyrosine kinase	CSK	1.542
O00442	RNA 3'-terminal phosphate cyclase	RTCA	1.540
Q9BWF3	RNA-binding protein 4	RBM4	1.534
P50897	Palmitoyl-protein thioesterase 1	PPT1	1.532
O75368	SH3 domain-binding glutamic acid-rich-like protein	SH3BGRL	1.525
Q03252	Lamin B2	LMNB2	1.521
Q01518	Adenylyl cyclase-associated protein 1	CAP1	1.517
Q9UH99	SUN domain-containing protein 2	SUN2	1.508
P04899	G protein subunit alpha i2	GNAI2	1.499
Q9BR76	Coronin 1B	CORO1B	1.497
Q01130	Serine/arginine-rich splicing factor 2	SRSF2	1.496
P26038	Moesin	MSN	1.494
Q9ULZ3	PYD and CARD domain containing	PYCARD	1.489
P48426	Phosphatidylinositol-5-phosphate 4-kinase type 2 alpha	PIP4K2A	1.484
P25774	Cathepsin S	CTSS	1.476
Q99439	Calponin 2	CNN2	1.475
Q12846	Syntaxin 4	STX4	1.472
P05362	Intercellular adhesion molecule 1	ICAM1	1.471
Q15833	Syntaxin binding protein 2	STXBP2	1.470
Q6PCB0	Von Willebrand factor A domain containing protein 1	VWA1	1.467
P29218	Inositol monophosphatase 1	IMPA1	1.461
P78344	Eukaryotic translation initiation factor 4 gamma 2	EIF4G2	1.460
O00499	Bridging integrator 1	BIN1	1.455
P61966	Adaptor related protein complex 1 sigma 1 subunit	AP1S1	1.449
O43707	Actinin alpha 4	ACTN4	1.449
P00568	Adenylate kinase 1	AK1	1.448
Q9GZP4	PITH domain containing 1	PITHD1	1.444
P27348	14-3-3 protein theta	YWHAQ	1.436
Q63HN8	Ring finger protein 213	RNF213	1.435
P53004	Biliverdin reductase A	BLVRA	1.432
P52907	F-actin-capping protein subunit alpha-1	CAPZA1	1.431
Q99873	Protein arginine methyltransferase 1	PRMT1	1.431
O00151	PDZ and LIM domain protein 1	PDLIM1	1.427
P61421	V-type proton ATPase subunit d1	ATP6V0D1	1.427
P16885	Phospholipase C gamma 2	PLCG2	1.427
Q6IBS0	Twinfilin actin binding protein 2	TWF2	1.423
Q9Y3Z3	SAM and HD domain containing deoxynucleoside triphosphate triphosphohydrolase 1	SAMHD1	1.418
P12814	Actinin alpha 1	ACTN1	1.417
Q15691	Microtubule associated protein RP/EB family member 1	MAPRE1	1.417
Q15637	Splicing factor 1	SF1	1.410
Q04206	RELA proto-oncogene, NF-kB subunit	RELA	1.408
O95352	Autophagy related 7	ATG7	1.402
Q9BZQ8	Protein Niban	FAM129A	1.400
O00743	Serine/threonine-protein phosphatase 6 catalytic subunit	PPP6C	1.399
P53999	Activated RNA polymerase II transcriptional coactivator p15	SUB1	1.398
Q92888	Rho guanine nucleotide exchange factor 1	ARHGEF1	1.396
Q52LJ0	Isoform 2 of Protein FAM98B	FAM98B	1.395
P49407	Arrestin beta 1	ARRB1	1.393
Q99733	Nucleosome assembly protein 1 like 4	NAP1L4	1.392
Q8WXF1	Paraspeckle component 1	PSPC1	1.390
Q9UL25	RAB21, member RAS oncogene family	RAB21	1.390
Q9BWM7	Sideroflexin 3	SFXN3	1.387
Q13464	Rho-associated protein kinase 1	ROCK1	1.385
P40121	Capping actin protein, gelsolin like	CAPG	1.379
O00267	Transcription elongation factor SPT5	SUPT5H	1.379
P09651	Heterogeneous nuclear ribonucleoprotein A1	HNRNPA1	1.378
P28482	Mitogen-activated protein kinase 1	MAPK1	1.378
Q15907	Ras-related protein Rab-11B	RAB11B	1.377
Q9UQE7	Structural maintenance of chromosomes protein 3	SMC3	1.376
Q8N1F7	Nuclear pore complex protein Nup93	NUP93	1.375
P63279	SUMO-conjugating enzyme UBC9	UBE2I	1.371
Q96FW1	OTU deubiquitinase, ubiquitin aldehyde binding 1	OTUB1	1.370
O95168	NADH dehydrogenase [ubiquinone] 1 beta subcomplex subunit 4	NDUFB4	1.367
P35659	Protein DEK	DEK	1.366
Q13045	FLII, actin remodeling protein	FLII	1.366
Q9BZZ5	Apoptosis inhibitor 5	API5	1.363
P14621	Acylphosphatase 2	ACYP2	1.358
Q9BT78	COP9 signalosome complex subunit 4	COPS4	1.356
Q14683	Structural maintenance of chromosomes protein 1A	SMC1A	1.354
O14617	Adaptor related protein complex 3 delta 1 subunit	AP3D1	1.344
Q92688	Acidic nuclear phosphoprotein 32 family member B	ANP32B	1.342
P36915	Guanine nucleotide-binding protein-like 1	GNL1	1.341
Q14204	Cytoplasmic dynein cytoplasmic 1 heavy chain 1	DYNC1H1	1.335
P62753	40S ribosomal protein S6	RPS6	1.334
Q9UHY7	Enolase-phosphatase E1	ENOPH1	1.334
Q13547	Histone deacetylase 1	HDAC1	1.332
O00160	Myosin IF	MYO1F	1.331
P06865	Beta-hexosaminidase subunit alpha	HEXA	1.331
P38919	Eukaryotic translation initiation factor 4A-III	EIF4A3	1.331
P19105	Myosin light chain 12A	MYL12A	1.331
P61970	Nuclear transport factor 2	NUTF2	1.330
P07951	Isoform 2 of Tropomyosin beta chain	TPM2	1.330
Q14980	Nuclear mitotic apparatus protein 1	NUMA1	1.323
O00182	Galectin 9	LGALS9	1.322
P38606	ATPase H+ transporting V1 subunit A	ATP6V1A	1.319
O95865	Dimethylarginine dimethylaminohydrolase 2	DDAH2	1.317
Q9Y2X3	NOP58 ribonucleoprotein	NOP58	1.316
Q9Y230	RuvB like AAA ATPase 2	RUVBL2	1.311
Q9Y6G9	Cytoplasmic dynein 1 light intermediate chain 1	DYNC1LI1	1.309
P09496	Clathrin light chain A	CLTA	1.308
A0AVT1	Ubiquitin like modifier activating enzyme 6	UBA6	1.307
P10644	cAMP-dependent protein kinase type I-alpha regulatory subunit	PRKAR1A	1.304
Q8WU39	Marginal zone B and B1 cell specific protein	MZB1	1.299
P62736	Actin, aortic smooth muscle	ACTA2	1.297
P62424	60S ribosomal protein L7a	RPL7A	1.297
O75431	Metaxin 2	MTX2	1.290
P47755	F-actin-capping protein subunit alpha-2	CAPZA2	1.289
O60493	Isoform 4 of Sorting nexin-3	SNX3	1.288
P19838	Nuclear factor kappa B subunit 1	NFKB1	1.287
P52565	Rho GDP-dissociation inhibitor 1	ARHGDIA	1.286
O43747	Adaptor related protein complex 1 gamma 1 subunit	AP1G1	1.286
O43399	Tumor protein D52 like 2	TPD52L2	1.282
Q16850	Cytochrome P450 family 51 subfamily A member 1	CYP51A1	1.281
Q8IWB7	WD repeat and FYVE domain containing protein 1	WDFY1	1.280
Q15046	Isoform Mitochondrial of Lysine--tRNA ligase	KARS	1.279
Q96KP1	Exocyst complex component 2	EXOC2	1.274
Q969V3	Nicalin	NCLN	1.272
P62995	Transformer 2 beta homolog (Drosophila)	TRA2B	1.263
Q9NSD9	Phenylalanyl-tRNA synthetase beta subunit	FARSB	1.260
Q9H3P7	Golgi resident protein GCP60	ACBD3	1.258
Q9UI12	ATPase H+ transporting V1 subunit H	ATP6V1H	1.257
Q9Y5X3	Sorting nexin 5	SNX5	1.256
Q13617	Isoform 2 of Cullin-2	CUL2	1.255
Q16539	Mitogen-activated protein kinase 14	MAPK14	1.254
Q9HA64	Fructosamine 3 kinase related protein	FN3KRP	1.253
P55769	NHP2-like protein 1	NHP2L1	1.253
P43034	Platelet activating factor acetylhydrolase 1b regulatory subunit 1	PAFAH1B1	1.250
Q15642	Cdc42-interacting protein 4	TRIP10	1.249
P55072	Transitional endoplasmic reticulum ATPase	VCP	1.247
P60842	Eukaryotic initiation factor 4A-I	EIF4A1	1.222
P10155	60 kDa SS-A/Ro ribonucleoprotein	TROVE2	1.200
Down-regulated proteins			
Q93088	Betaine-homocysteine S-methyltransferase 1	BHMT	0.382
P00326	Alcohol dehydrogenase 1C	ADH1C	0.480
P02743	Serum amyloid P-component	APCS	0.485
P31512	Dimethylaniline monooxygenase [N-oxide-forming] 4	FMO4	0.506
P20962	Parathymosin	PTMS	0.515
Q9BSE5	Agmatinase, mitochondrial	AGMAT	0.522
O75891	Cytosolic 10-formyltetrahydrofolate dehydrogenase	ALDH1L1	0.525
Q8IWW8	Hydroxyacid-oxoacid transhydrogenase, mitochondrial	ADHFE1	0.525
Q04828	Aldo-keto reductase family 1 member C1	AKR1C1	0.533
P01859	Ig gamma-2 chain C region	IGHG2	0.536
P00325	Alcohol dehydrogenase 1B	ADH1B	0.543
Q96F10	Diamine acetyltransferase 2	SAT2	0.548
P36871	Phosphoglucomutase-1	PGM1	0.548
P45954	Short/branched chain specific acyl-CoA dehydrogenase, mitochondrial	ACADSB	0.549
P54840	Glycogen (starch) synthase, liver	GYS2	0.557
O95563	Mitochondrial pyruvate carrier 2	MPC2	0.559
Q9UBQ7	Glyoxylate reductase/hydroxypyruvate reductase	GRHPR	0.561
P07108	Acyl-CoA-binding protein	DBI	0.564
P06133	UDP-glucuronosyltransferase 2B4	UGT2B4	0.574
P00167	Cytochrome b5	CYB5A	0.576
Q9UI17	Dimethylglycine dehydrogenase, mitochondrial	DMGDH	0.591
P16930	Fumarylacetoacetase	FAH	0.594
P27338	Amine oxidase [flavin-containing] B	MAOB	0.594
P20813	Cytochrome P450 2B6	CYP2B6	0.599
P30039	Phenazine biosynthesis-like domain-containing protein	PBLD	0.601
P00505	Aspartate aminotransferase, mitochondrial	GOT2	0.602
O43175	D-3-phosphoglycerate dehydrogenase	PHGDH	0.604
Q15493	Regucalcin	RGN	0.604
Q6NVY1	3-hydroxyisobutyryl-CoA hydrolase, mitochondrial	HIBCH	0.605
O60656	UDP-glucuronosyltransferase 1-9	UGT1A9	0.607
P49326	Dimethylaniline monooxygenase [N-oxide-forming] 5	FMO5	0.609
Q7Z4W1	L-xylulose reductase	DCXR	0.609
Q14353	Guanidinoacetate N-methyltransferase	GAMT	0.615
P08684	Cytochrome P450 3A4	CYP3A4	0.619
Q02252	Methylmalonate-semialdehyde dehydrogenase [acylating], mitochondrial	ALDH6A1	0.627
P34896	Serine hydroxy methyltransferase, cytosolic	SHMT1	0.630
O60701	UDP-glucose 6-dehydrogenase	UGDH	0.634
Q16762	Thiosulfate sulfurtransferase	TST	0.636
P47989	Xanthine dehydrogenase/oxidase	XDH	0.639
P24462	Cytochrome P450 3A7	CYP3A7	0.647
P30084	Enoyl-CoA hydratase, mitochondrial	ECHS1	0.651
Q9Y617	Phosphoserine aminotransferase	PSAT1	0.655
P28072	Proteasome subunit beta type-6	PSMB6	0.655
Q969Z3	Mitochondrial amidoxime reducing component 2	MARC2	0.658
Q02928	Cytochrome P450 4A11	CYP4A11	0.660
Q14914	Prostaglandin reductase 1	PTGR1	0.662
P24298	Alanine aminotransferase 1	GPT	0.663
P42126	Enoyl-CoA delta isomerase 1, mitochondrial	ECI1	0.667
Q96HR9	Receptor expression-enhancing protein 6	REEP6	0.669
Q68CK6	Acyl-coenzyme A synthetase ACSM2B, mitochondrial	ACSM2B	0.669
P05177	Cytochrome P450 1A2	CYP1A2	0.672
Q9H488	GDP-fucose protein O-fucosyltransferase 1	POFUT1	0.673
P09327	Villin-1	VIL1	0.674
Q9H477	Ribokinase	RBKS	0.675
P02763	Alpha-1-acid glycoprotein 1	ORM1	0.676
P06331	immunoglobulin heavy variable 4-34	IGHV4-34	0.677
P51857	3-oxo-5-beta-steroid 4-dehydrogenase	AKR1D1	0.678
P49419	Alpha-aminoadipic semialdehyde dehydrogenase	ALDH7A1	0.679
Q14749	Glycine N-methyltransferase	GNMT	0.679
P42765	3-ketoacyl-CoA thiolase, mitochondrial	ACAA2	0.681
Q4G0N4	NAD kinase 2, mitochondrial	NADK2	0.685
Q96LJ7	Dehydrogenase/reductase SDR family member 1	DHRS1	0.687
Q687X5	Metalloreductase STEAP4	STEAP4	0.688
Q9Y2V2	Calcium-regulated heat stable protein 1	CARHSP1	0.693
Q99447	Ethanolamine-phosphate cytidylyltransferase	PCYT2	0.693
P15090	Fatty acid-binding protein, adipocyte	FABP4	0.696
Q9NPJ3	Acyl-coenzyme A thioesterase 13	ACOT13	0.700
Q9H8H3	Methyltransferase-like protein 7A	METTL7A	0.701
P51648	Fatty aldehyde dehydrogenase	ALDH3A2	0.701
Q16822	Phosphoenolpyruvate carboxykinase (GTP), mitochondrial	PCK2	0.702
P19022	Cadherin-2	CDH2	0.708
P27144	Adenylate kinase 4, mitochondrial	AK4	0.708
O75381	Peroxisomal membrane protein PEX14	PEX14	0.709
Q9UL12	Sarcosine dehydrogenase, mitochondrial	SARDH	0.711
P01023	Alpha-2-macroglobulin	A2M	0.716
Q8IVS8	Glycerate kinase	GLYCTK	0.719
P26440	Isovaleryl-CoA dehydrogenase, mitochondrial	IVD	0.722
Q86YB7	Enoyl-CoA hydratase domain-containing protein 2, mitochondrial	ECHDC2	0.722
P27169	Serum paraoxonase/arylesterase 1	PON1	0.728
P61604	10 kDa heat shock protein, mitochondrial	HSPE1	0.729
P50225	Sulfotransferase 1A1	SULT1A1	0.733
P05089	Arginase-1	ARG1	0.734
O75521	Enoyl-CoA delta isomerase 2, mitochondrial	ECI2	0.735
Q99436	Proteasome subunit beta type-7	PSMB7	0.735
P22760	Arylacetamide deacetylase	AADAC	0.737
P16152	Carbonyl reductase [NADPH] 1	CBR1	0.739
P21912	Succinate dehydrogenase [ubiquinone] iron-sulfur subunit, mitochondrial	SDHB	0.740
P43155	Carnitine O-acetyltransferase	CRAT	0.742
P10599	Isoform 2 of Thioredoxin	TXN	0.746
P16219	Short-chain specific acyl-CoA dehydrogenase, mitochondrial	ACADS	0.748
Q9Y2Q3	Glutathione S-transferase kappa 1	GSTK1	0.749
Q9BUP3	Oxidoreductase HTATIP2	HTATIP2	0.749
P62266	40S ribosomal protein S23	RPS23	0.753
O75191	Xylulose kinase	XYLB	0.755
P30613	Pyruvate kinase PKLR	PKLR	0.758
Q9NQR4	Omega-amidase NIT2	NIT2	0.758
O94855	Protein transport protein Sec24D	SEC24D	0.760
P83111	Serine beta-lactamase-like protein LACTB, mitochondrial	LACTB	0.761
Q6UWY5	Olfactomedin-like protein 1	OLFML1	0.762
Q86SX6	Glutaredoxin-related protein 5, mitochondrial	GLRX5	0.763
Q14624	Inter-alpha-trypsin inhibitor heavy chain H4	ITIH4	0.774
Q9UIJ7	GTP:AMP phosphotransferase AK3, mitochondrial	AK3	0.775
P01764	Ig heavy chain V-III region 23	IGHV3-23	0.788
Q92597	Protein NDRG1	NDRG1	0.789
P07306	Asialoglycoprotein receptor 1	ASGR1	0.790
P02461	Collagen alpha-1(III) chain	COL3A1	0.794
P34897	Serine hydroxy methyltransferase, mitochondrial	SHMT2	0.795
Q86TX2	Acyl-coenzyme A thioesterase 1	ACOT1	0.800
Q00796	Sorbitol dehydrogenase	SORD	0.802
Q16134	Electron transfer flavoprotein-ubiquinone oxidoreductase, mitochondrial	ETFDH	0.803
Q9UF12	Probable proline dehydrogenase 2	PRODH2	0.806
Q00765	Receptor expression-enhancing protein 5	REEP5	0.809
Q96LZ7	Regulator of microtubule dynamics protein 2	RMDN2	0.833
P08603	Complement factor H	CFH	0.833

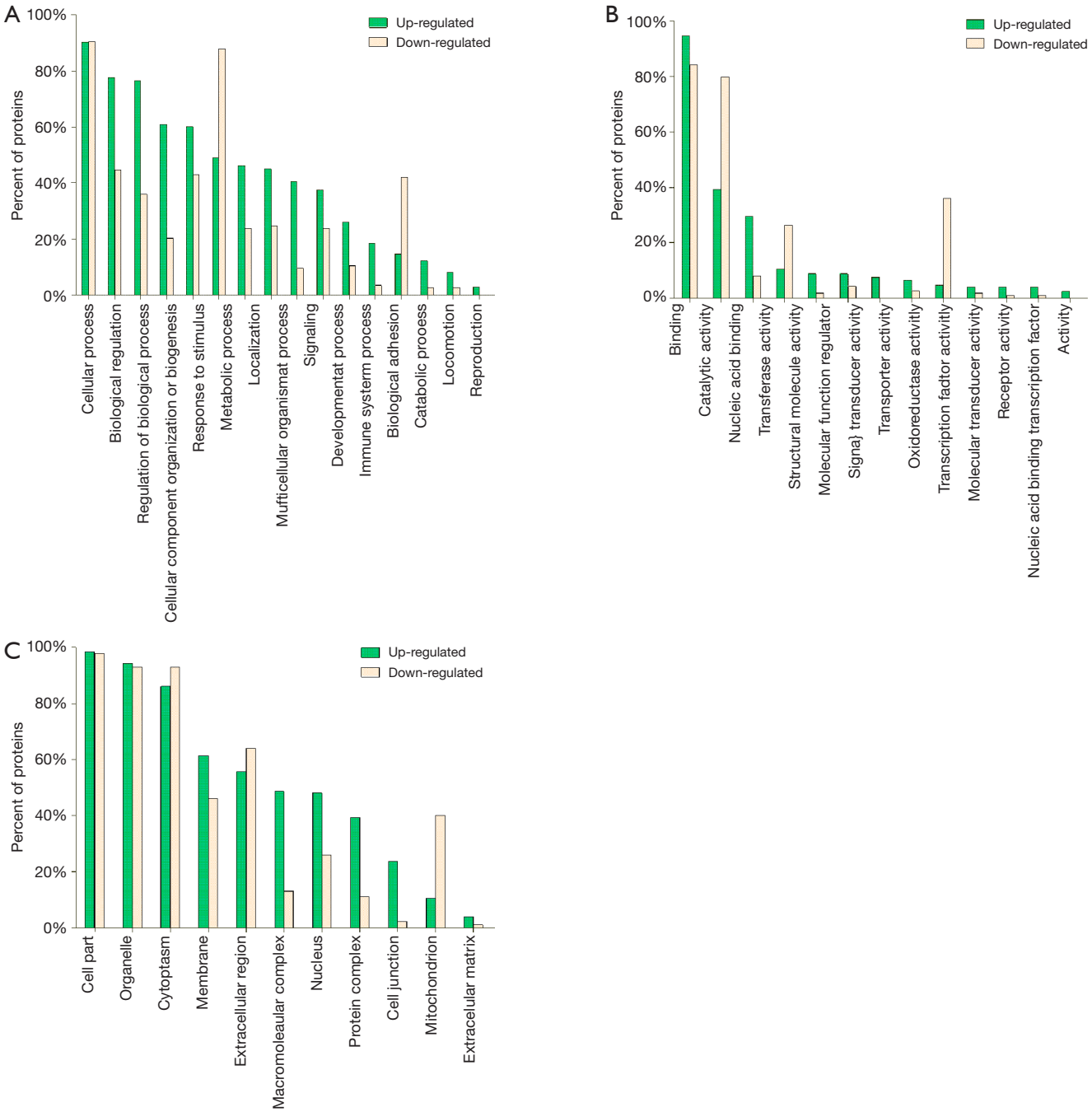

Figure S2 Gene ontology analysis of the DEPs identified by iTRAQ. The identified proteins were categorized into biological process (A), molecular function (B), and cell component (C), analyzed by PANTHER Classification System (http://www.pantherdb.org/). % means the number of the proteins found in the specific term against the total number of the up-regulated or down-regulated proteins.

Table S3 The DEPs involved in the GO term of immune system process

Identified proteins	Number	Fold enrichment	P	Details
Up-regulated DEPs	45	2.62	1.10E-05	NFKB1, MAPK1, MAPK14, VCAM1, ICAM1, KARS, HMOX1, FKBP1A, ITGB3, HLA-DPA1, ARPC3, LGMN, OTUB1, TAP1, GRB2, PAFAH1B1, CNN2, TROVE2, AP3D1, ACTG1, ATG7, DYNC1H1, CLTA, MSN, PIP4K2A, RPS6, STXBP2, PLCG2, LGALS9, RELA, SAMHD1, AP1S1, PYCARD, PPBP, ACTN1, PTPRC, CORO1A, FCGR3A, CSK, CAPZA2, CAPZA1, AP1G1, CTSS, GNL1, ROCK1
Down-regulated DEPs	12	1.07	4.62E-01	PSMB6, APCS, IGHV4-34, IGHG2, SHMT2, IGHV3-23, SEC24D, PSMB7, NDRG1, GLRX5, CFH, PTMS

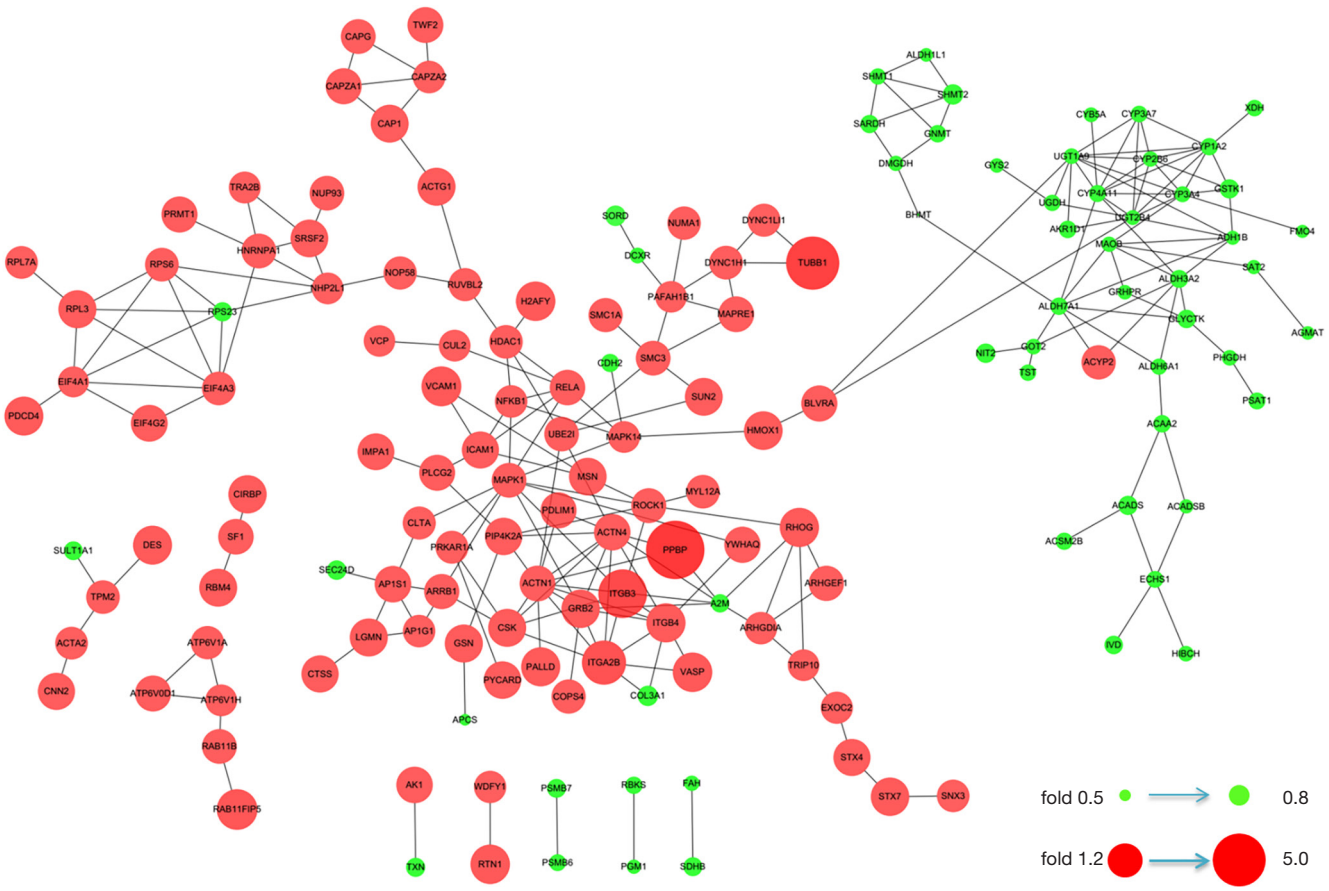

Figure S3 The reconstructed PPI network in Cytoscape. Red nodes: up-regulated proteins; green nodes: down-regulated proteins. The size of the nodes represents the protein expression level.

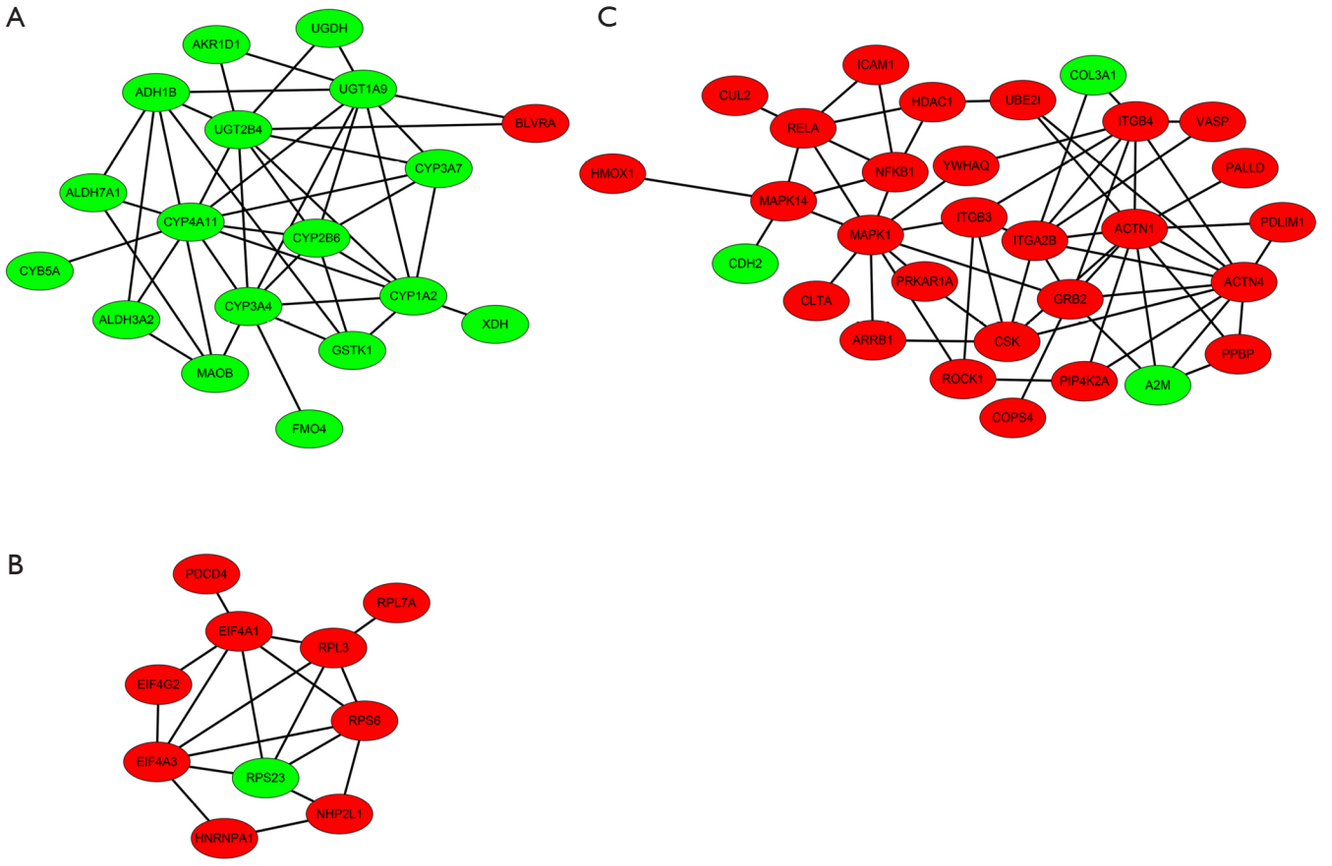

Figure S4 The significant modules from the PPI network with MCODE score >4 and node >10. (A) Module 1; (B) module 2; (C) module 3. The node stands for the protein (gene); red nodes were up-regulated proteins; gray nodes stands were down-regulated proteins.

Table S4 The enriched pathways identified in the functional modules

PANTHER pathways	Counts	Fold enrichment	P
Module 1			
Bupropion degradation	1	>100	8.58E-04
Purine metabolism	1	>100	5.99E-03
Adenine and hypoxanthine salvage pathway	1	>100	5.99E-03
5-hydroxytryptamine degradation	3	>100	8.10E-07
Adrenaline and noradrenaline biosynthesis	1	38.84	2.54E-02
Dopamine receptor mediated signaling pathway	1	19.75	4.94E-02
Module 2			
Toll receptor signaling pathway	4	46.6	2.73E-04
Blood coagulation	3	44.62	6.90E-03
B cell activation	4	38.84	5.60E-04
Integrin signalling pathway	10	36.41	1.66E-11
T cell activation	4	29.13	1.73E-03
Parkinson disease	4	27.96	2.03E-03
Ras pathway	3	27.59	2.84E-02
FGF signaling pathway	4	22.55	4.68E-03
CCKR signaling map	5	20.2	7.24E-04
EGF receptor signaling pathway	4	20.12	7.28E-03
Inflammation mediated by chemokine and cytokine signaling pathway	5	13.39	5.18E-03

No enriched pathway was found in module 3.